Dispersion and Solvation Effects on the Structure and Dynamics of N719 Adsorbed to Anatase-Titania (101) Surfaces in Room-Temperature Ionic Liquids: An *ab initio* Molecular Simulation Study

Aaron Byrne,[1,2,3] Niall J. English,[1,4,a)] Udo Schwingenschlögl[5] and David. F. Coker[2,3,6,b)]

[1]*School of Chemical and Bioprocess Engineering,* [2]*School of Physics,*
[3]*Complex Adaptive Systems Laboratory,*
University College Dublin, Belfield, Dublin 4, Ireland.

[4]*The SFI Strategic Research Cluster in Solar Energy Conversion*

[5]*PSE Division, KAUST, Thuwal 23955-6900, Saudi Arabia.*

[6]*Dept. of Chemistry, Boston University, Boston, USA.*

Abstract

Ab initio, Density Functional Theory (DFT)-based molecular dynamics (MD) has been carried out to investigate the effect of explicit solvation on the dynamical and structural properties of a [bmim][NTf_2] room-temperature ionic liquid (RTIL), solvating a N719 sensitising dye adsorbed onto an anatase-titania (101) surface. The effect of explicit dispersion on the properties of this dye-sensitised solar cell (DSC) interface has also been studied. Upon inclusion of dispersion interactions in simulations of the solvated system, the average separation between the cations and anions decreases by 0.6 Å, the mean distance between the cations and the surface decreases by about 0.5 Å and the layering of the RTIL is significantly altered in the first layer surrounding the dye, with the cation being on average 1.5 Å further from the centre of the dye. Inclusion of dispersion effects when a solvent is not explicitly included (to dampen longer range interactions) can result in unphysical "kinking" of the adsorbed dye's configuration. The inclusion of solvent shifts the HOMO and LUMO levels of the titania surface by +3 eV. At this interface, the interplay between the effects of dispersion and solvation combine in ways that are often subtle, such as enhancement or inhibition of specific vibrational modes.

Corresponding authors. Email: [a)] niall.english@ucd.ie, [b)] coker@bu.edu

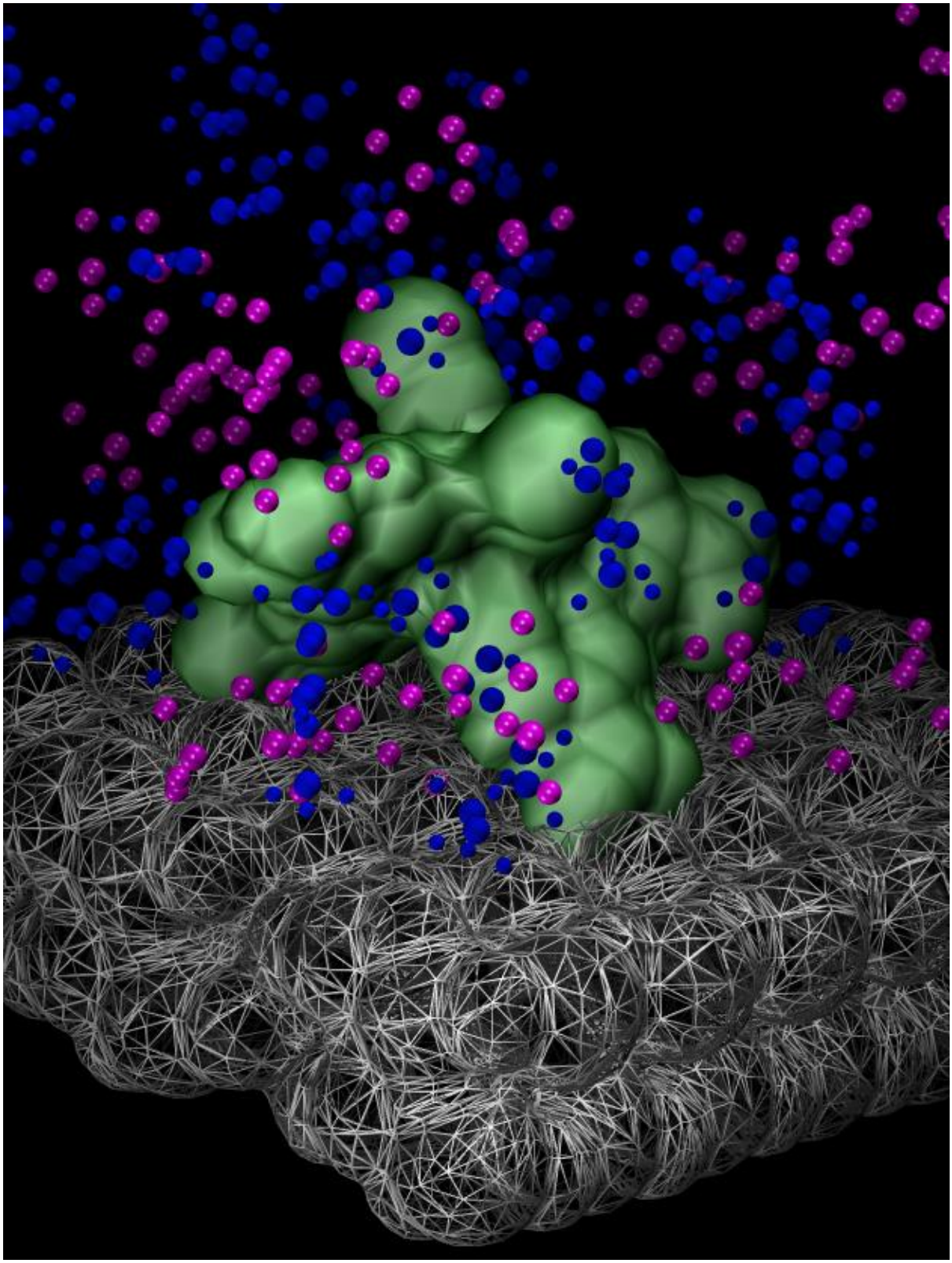

Above: Representative configuration from simulations of a dye-sensitised solar cell interface with a room temperature ionic liquid electrolyte. Shown in the centre in green is the light absorbing dye, whilst the titania surface is depicted by metallic spheres and the atoms of the room-temperature ionic liquid cations (anions) are shown in blue (magenta).

1. Introduction

Dye-sensitised solar cells (DSCs) are a form of solar technology whereby the optical band gap of the semiconductor is bridged by a light-absorbing dye. These devices consist of a sensitising dye, N719 being one of the most commonly studied, adsorbed onto a mesoporous semiconductor electrode, usually TiO_2. In order for a DSC to function, it needs to have its charge continually replenished, and it is therefore necessary to have some form of redox electrolyte (usually I^-/I_3^- in an organic solvent) as the third primary component. This allows the hole to transfer from the dye to the electrolyte, while electrons injected into the semiconductor move through it into the external circuit, till these charge carriers ultimately recombine at the cathode, completing the circuit. DSCs are set to become strong contenders to silicon-based photovoltaics and other less renewable forms of energy generation.[1,2] An essential component of DSC's appeal lies in the fact that they can be manufactured cheaply and do not require high-purity materials,[3] unlike more traditional silicon-based photovoltaic technology. Despite over 20 years of research into these promising DSC devices, there is still some uncertainty concerning the precise underlying physical and chemical processes.[4]

Ultimately, the deployment of any form of solar technology in the field requires it to be cost-competitive over its lifecycle. Being able to extend that lifecycle indefinitely through the replacement of a volatile electrolyte with low volatility room-temperature ionic liquids (RTILs) offers much promise.[5-7] RTILs are molten salts, composed of molecular cations and anions, which have by definition a melting point less than 100^{o}C. They exhibit liquid-like electrical properties but solid-like physical ones, including low flammability, volatility and toxicity.[8] In effect, the inclusion of RTILs in DSCs as the electrolyte removes many of the drawbacks of the heterogeneous nature of more traditional DSCs, making them more stable and significantly improving their lifetimes.[6] This forms a strong imperative for studying the effects RTILs have on the DSC.

The exact process of adsorption of the N719 dye onto the TiO_2 surface is still debated, as different experimental[9-11] and theoretical studies[12,13] have suggested differing mechanisms and binding sites; for a more complete account, see the review by Lee *et al*.[9] The N719 dye has four carboxylate groups, through which it can coordinate with binding possible to one, two or three of these sites. For each binding site, there are also four possible chemisorption configurations: monodentate, bidentate bridging, bidentate chelating and pseudo-bridging, as

well as the two physisorption configurations of single hydrogen- (H-) bonded and double H-bonded. These different binding possibilities are presented in Fig. 1.

[insert Fig. 1 here]

Taking into account surface hydroxyl groups that arise, for example, from binding of the dye to the TiO_2 surface is important to fully understand the binding modes; for instance, a study by Schiffman *et al.*[12] has shown that the most stable configuration of the dye on anatase, when surface protons are taken into account, possesses two carboxylate groups with a mixed bidentate bridging / monodentate configuration. For this reason, we used this configuration as the starting point for our study. In Fig. 2, for instance, we present an example configuration from our simulations in which the left-side binding is bidentate in character, with two oxygen atoms of the dye binding to two different titanium atoms in the slab, whereas on the right-side, monodentate binding is featured, wherein only one oxygen atom is bound to a titanium atom in the slab.

[insert Fig. 2 here]

Often, computational studies of DSCs are forced to ignore the effect of the solvent on the interface, and assume a continuum or gas-phase model, due to the significant computational cost of simulating a liquid explicitly. However, including a detailed molecular description of the solvent in complex systems can reveal markedly different behaviour, as for instance in the work of Bandaru *et al.*[14] or de Almeida *et al.*[15] In the former case, it was found that the accurate modelling of the structure of a ruthenium catalyst required explicit inclusion of THF solvent molecules, while the latter study found that the near infra-red absorption spectra of bis(hexafluoroacetylacetonate) copper(II) was strongly dependent on the surrounding pyridine solvent. In particular for the TiO_2 system, Mosconi *et al.*[16] found recently using Car-Parrinello molecular-dynamics (MD) calculations that the explicit inclusion of a solvent (water and acetonitrile) led to deprotonation of the sensitising dye, with significant structural differences, and further, the conduction band of TiO_2 was upshifted by 0.3 eV in the case of acetonitrile.[16] Similarly, the addition of explicit dispersion corrections[17,18] to DFT functionals can significantly alter both the behaviour of room-temperature ionic liquids[19] and titania interfaces.[20] For instance, Izgorodina *et al.* found that the widely used B3LYP-D hybrid functional fares poorly on tests involving ionic liquids, with a mean average deviation of 22.3 kJ mol^{-1} from their MP2 benchmark,[19] whilst Castells

et al. have shown that the interaction energy of a titania surface in contact with helium is heavily dependent on the dispersion methodology employed. [20]

As it becomes feasible to perform *ab initio* MD studies of complex systems with on the order of a thousand atoms[21] using linear-scaling DFT methods,[22,23] careful study of the often significant influence of solvation and dispersion effects can now be undertaken. In the present study, we carry out a series of *ab initio* MD simulations demonstrating the complex interplay that occurs when dispersion effects are employed with an explicit solvent and how the lack of a reliable description of either one of these effects can alter the fundamental behaviour of the dye-electrolyte-semiconductor interface considerably. Our goal here is to characterise the structural stability, as well as dynamical and structural properties of such interfaces and explore the influence of incorporating polarization effects in *ab initio* MD treatments of these complex systems.

2. Methodology

The sensitising dye used in our simulations was N719: cis-di(thiocyanato)-bis(2,2'-bipyridl-4-carboxylate-4'-carboxylic acid)-ruthenium(II), with no counter-ions and two surface bound protons that result from carboxylic acid group dissociation during dye surface binding. Previous work by De Angelis *et al*.[24] has shown this to be a realistic representation of N719. For example, they found that including bulky tert-butyl alcohol (TBA) counter-ions has only the slight effect of downshifting the conduction band of the TiO_2 by 0.03 eV.[24] In our initial configuration the dye was chemically adsorbed to the TiO_2 surface through two carboxylate groups, one of which was bidentate bridging, and the other monodentate. This starting adsorbed configuration of the dye is similar to the configuration labelled as I_1 in the study of Schiffmann *et al*,[12] in which they found it to be the most stable when surface protons were taken into account (as we have in this present study, cf. Fig 2). Martsinovich *et al*. have suggested that the TiO_2 slab interface models can be relatively insensitive to slab thickness,[25] however here we have chosen to constrain the bottom-most layer of the titania to provide a more realistic simulation of a thicker slab, especially considering that due to the use of periodic boundary conditions in our RTIL – interface system, the bottom of the slab would be in contact with the top layer of the strongly interacting ionic solvent. The RTIL used in these simulations was twelve cation-anion pairs of 1-butyl-3-methylimidazolium bis(trifluoromethylsulphonyl)imide, consisting of 480 atoms in total. The starting configuration for the liquid was one that had been relaxed via classical MD in previous

work[26], which found the layering effects in this RTIL to be important but that they were localised only in the region out to ~1 nm from the interface. Although the liquid in that simulation[26] surrounded a different semiconductor (mica), it gave a reasonable starting point once care was taken to avoid close contacts between fluid atoms and the dye or anatase by removing select liquid molecules. As outlined below our simulation cell is significantly thicker than the 1nm layered region so we expect the effects of layering to be damped out before we encounter the periodic image of the TiO_2 slab in the z-direction, and also to be significantly disrupted by the presence of the surface adsorbed dye molecule.

The semiconductor substrate consisted of an anatase titania surface $(TiO_2)_{96}$ (288 atoms), periodic in x and y and exposing two parallel (101) surfaces perpendicular to the *z*-axis, of 2.3 x 2.1 nm^2 surface area. Bulk anatase has lattice vectors $a_0=b_0=$ 3.776 Å and c_0=9.486 Å and a symmetry group I41/AMD. De Angelis *et al.*[13] found the difference in the optical band gap between the (001) and (101) surfaces to be essentially negligible, and the (101) surface was therefore chosen so as to enable us to check for consistency with other simulations.[12,27] The periodicity along *z* (L_z =2.6 nm) is such to leave a gap of 1.6 nm between the periodic replicas of the titania slab. This space is sufficient to accommodate a dye molecule (N719-2H/0TBA), a Ru-based metallo-organic species, and, in the case of explicit solvent, to surround it with 12 $[bmim]^+[NTf_2]^-$ ion pairs. Fig. 3 shows such a cell containing a solvated dye and surface. The DSC with explicit solvent used in this study is composed of 827 atoms and has 4300 valence electrons. In the *in vacuo* case, there were 347 atoms and 2530 valence electrons.

[insert Fig. 3 here]

The simulations were carried out using Born-Oppenheimer Molecular Dynamics (BOMD), as implemented in the CP2K[28-34] software package. The DFT calculations employed the generalised gradient approximation (GGA) using the PBE[35] exchange-correlation functional, and triple zeta basis sets. A cut-off of 400 Ry was used for all *ab initio* MD simulations. Geometry optimisation was first performed for the titania slab and then for the slab with N719 adsorbed onto it. This configuration provided the initial conditions for the unsolvated calculations outlined below. Next the system was surrounded with 12 RTIL anion-cation pairs and a brief equilibration run of the solvated system, without explicit Grimme dispersion, was performed involving an *ab initio* MD calculation for 300 fs with a 1

fs time-step until the configurational energy of the system fluctuated around some value indicating stability. This configuration provided the initial condition for our solvated calculations.

To enable accurate comparisons and study how the inclusion of dispersion and/or solvation affects influence the structure and dynamics of this interface, four simulations were run using the initial conditions described above. For the simulations of systems including explicit dispersion effects, the Grimme D3 dispersion correction[18] was added to the functional. Systems I and II were obtained by simply running the optimized unsolvated initial configuration displayed in Fig. 4a. for 8.5ps, with and without dispersion corrections respectively. Systems III and IV were obtained by running calculations for 8.5ps after inclusion of solvent and initial equilibration again with and without inclusion of dispersion interactions respectively. All calculations were run with BOMD in the NVT ensemble at T=300K using a 1 fs time-step. The temperature was fixed by coupling the systems to a Nosé-Hoover[36] thermostat with a time period of 0.15 ps and the virial-estimated[37] pressure was found to average to ~1 atm.

[insert Fig. 4 here]

Velocity autocorrelation functions (VACF) were calculated for specific atoms of interest for each of the four systems and then Fourier-transformed to give power spectra.[37,46] As has been noted in previous work,[38] autocorrelation functions derived from *ab initio* MD are prone to 'miss' lower frequency features due to the prohibitive computational costs of running the simulations for long enough times. In this work, the largest correlation time considered was 7.5 ps which gives reasonably averaged results for frequencies down to ~50 cm^{-1} allowing us to study the vibrational dynamics of the slowly-relaxing ionic liquid. Different pair distribution functions[37], $g_{ij}(r)$, averaged over an interval of 1000 time-steps were also calculated for each system, 'at the outset' between 1 and 2 ps and then later between 7.5 and 8.5 ps, enabling us to explore changes to the structure of the interface for each system as a function of relaxation time. As discussed below, these structural changes were found to be very relevant when explicit dispersion corrections were included.

RTILs are known for both their extremely long-range interfacial layering and relaxation times,[26,39] that can be on the order of hundreds of nanoseconds, if not milliseconds. Although the *ab initio* study reported here of multiple systems consisting of hundreds of

atoms, with thousands of electrons, which we have followed for thousands of time steps is at the forefront of what is currently computationally feasible, it is still far beyond current capabilities to reach typical relaxation times of RTIL systems with this level of detailed description. Indeed, here we are more concerned with capturing the local relaxation behaviour of the composite interface involving the dye, semiconductor and RTIL electrolyte and on how dispersion interactions influence this structure, rather than focusing on the bulk RTIL properties, which are better explored by other techniques and have been studied elsewhere.[26,40-42]

The combined density of states of the titanium and oxygen atoms comprising the anatase were computed for each of the systems under study from their respective geometries after the 8.5ps of dynamics.

3. Results & Discussions

The results presented below explore the influence of explicit inclusion of solvent and dispersion interactions by comparing four separate *ab initio* simulations:

System I: semiconductor and dye *in vacuo*,

System II: semiconductor and dye *in vacuo* and with dispersion interactions,

System III: semiconductor, dye and RTIL,

System IV: semiconductor, dye and RTIL with dispersion interactions.

3.1 Solvation effects on structure

A prominent feature of note in our simulation of System I, the bare semiconductor – dye interface in which we ignore dispersion interactions, is the observation that the final configuration displayed in Fig. 4b has changed dramatically from the initial one presented in Fig. 4a over the timescale of our simulation. Specifically, we see that one of the non-binding carboxylic acid groups begins to bend towards the TiO_2 surface after about 3.5 ps, forming a hydrogen bond with an oxygen atom in the surface. This can also be seen from examination of the pair distribution functions for the hydrogen atoms of the dye and the oxygen atoms of TiO_2 before and after this rearrangement takes place as presented in Fig. 5a. The combination of chemical and physical adsorption observed here resembles closely the triply bound optimised geometry found in De Angelis *et al*.[27]

In the studies presented here we distinguish the chemisorption binding sites like the mono-dentate and bi-dentate carboxylate attachments to the surface titanium atoms and the physisorption binding sites that involve H-bonding between O-H groups on the dye and O-atoms on the surface or between surface hydroxyl groups H-bonding to O-atoms of the dye molecule.

[insert Fig. 5 here]

In our simulations containing an explicit solvent however, we saw that the presence of the solvent stabilised the structure of the dye molecule and the bending towards the surface did not take place. The pair distribution function presented in Fig. 5b shows how the early configuration changes little over the course of the simulation. This is in stark contrast with the significant structural changes seen in the unsolvated simulations as the dye relaxes towards a different local energy minima.

The fact that we see a re-arrangement of the dye's binding sites for systems *in vacuo* within the order of a few picoseconds helps to rationalise why it has been difficult to characterise definitively from spectroscopy the exact binding mechanism present for this interface.[9]

3.2 Dispersion effects on structure

Our System II simulations of the bare semiconductor – dye interface, which now include the influence of dispersion interactions using the Grimme D3 correction terms,[18] were initialized in exactly the same configuration (see Fig 4a) as the simulations of System I outlined above. We find that the long-range electron correlation effects, incorporated semi-empirically in the Grimme dispersion corrections strongly influence in the local structure and dynamics of the bare interface system. Within the first 1.5 ps of this simulation, the adsorbed dye molecule begins bending down towards the TiO_2 surface in a manner similar to what we observed with System I in the absence of dispersion interactions, but there are some significant differences. This reorganization can be seen readily in Figs. 6a, b, and c, which show side views of the simulated bare interface System II including dispersion interactions at t=0, 1.5 and 8 ps, respectively. Comparing Fig. 4a with Fig. 6a we see that our view in figure 6 looks directly at the side with the initial bi-dentate binding carboxylate in the foreground. The two initially surface bound hydrogen atoms are coloured black in all the panels of Fig. 6. The initially surface bound hydrogen on the left in Fig. 6a is furthest from our viewpoint and

some 2.5 Å from the mono-dentate binding carboxylate, while the surface bound hydrogen on the right is closest to our viewpoint. From Fig. 6b we see that with the Grimme dispersion interactions turned on there are two concerted surface rearrangements occurring in the first 1.5ps: The carboxylic acid group on the far right is reaching down and beginning to H-bond with a surface O-atom. However, at the same time, on the far left we see that the initial mono-dentate surface bound carboxylate has picked off the distant, formerly surface hydrogen, *i.e.* a proton transfer event from the surface to the dye has occurred, and the newly formed carboxylic acid group has detached entirely from the surface. The result of these concerted processes (H-bonding physisorption on the right and chemi-desorption and carboxylate protonation on the left) "marches" the entire dye complex significantly to the right about 2.76 Å from its initial position and causes the dye molecule to become significantly internally distorted. From Fig. 6c we see that by 8.0ps these strong distorting forces have partially up-rooted the bi-dentate binding anchor site closest to us, causing it to twist towards a Ti-atom further to the right but it is now only a mono-dentate attachment.

[insert Fig. 6 here]

This interface reconstruction changes both the chemical environment and physical structure of the dye. In effect, the inclusion of longer-range dispersion interactions has changed the most stable binding configuration of the dye from a doubly bound, mixed bi-dentate/mono-dentate configuration to a mono-dentate binding configuration with a single H-bond.

Although both Systems I and II bend towards the anatase surface, albeit in significantly different ways, it is clear that of the four systems studied, System II is the least physically realistic representation; in part, this is due to envisaged substantial energy barriers for its rearrangement process (cf. Fig. 6) and the short time frames over which they occur.

3.3 Dispersion effects on RTIL layering

By comparing the properties of systems III and IV we can study how including dispersion interactions influences the arrangement of the cations and^{-} anions, which comprise the RTIL. Looking at the intermolecular pair distribution functions for the centre of mass of the anions and cations with the Ti-atoms in the surface, with and without explicit treatment of dispersion interactions (see Fig. 7), one notes that when dispersion interactions are included

explicitly the cations relax to a state in which they are on average closer to the surface by 0.5 Å. This effect is not observed for the anions.

[insert Figs. 7 here]

The layer structure of the cations and anions around the dye molecule exhibit dramatic differences depending on whether the dispersion effects are included explicitly or not. The depiction of this layering is shown in Figs. 8a,8b,8c,8d. The layering of the anion around the dye in the system with dispersion displays a distinct void in the region between 8 and 9 Å, which is not present when dispersion corrections are absent. Likewise the distribution of cations around the dye also undergoes a dramatic re-ordering, where in the early (later) stages of the simulation the nearest neighbour distance is 1 Å closer together (1.5 Å further away), with explicit dispersion corrections than without.

[insert Figs. 8 here]

As shown in Figs. 8e and 8f the pair distribution functions for intermolecular distances between bmim cations and NTf_2 anions show evidence that with explicit treatment of dispersion interactions the solvents' cations and anions are attracted towards each other more strongly than in the absence of explicit treatment of dispersion. This effect is quite significant with the nearest neighbour peaks shifting to closer distances by as much as ~0.6 Å. This is to be expected, given the inclusion of dispersion effects through an attractive Grimme C^6 empirical term.

3.4 Dynamics of the binding modes

The vibrational power spectra calculated from the VACF of the carboxylic acid carbon atom labelled C_a can be found in Fig. 13a. For systems I and II, we see that the expected C=O stretch mode of a carboxylic acid (*circa* 1720 cm^{-1}) is conspicuously absent for the two solvated systems III and IV. The inclusion of the solvent does seem to enhance a peak around 750 cm^{-1}; experimental data does not go down this low, unfortunately. The spectra depicted in Fig. 13b are for the carboxylate carbon labelled C_b, and again we see that the expected mode of 1600 cm^{-1} for an anti-symmetric COO^- stretching of carboxylate is almost completely damped out in the systems involving solvent. System II is also missing this mode, and this is thought to be due to the modification (and mollification) to the

monodentate-bridging mode via proton transfer (*vide supra* – cf. section 3.2). Also, as in the case of C_a, a vibration around 750 cm^{-1} is enhanced.

C_c is the carbon atom belonging to the bidentately-bound carboxylate, with its spectra shown in Fig. 13c. For this carbon atom, we see more "structure" to its spectra, indicating that it has more vibrational modes. Again, due to the alteration to the binding mode for system II, we do not see a peak around 1470 cm^{-1}, but we do note some evidence of structure at the extreme lower end of the spectrum. In the solvated cases, we see an additional peak around 1330 cm^{-1}, and the peaks around 760 cm^{-1} also appear to be significantly damped when compared to system I. The remaining carbon of interest (labelled C_d) belongs to the carboxylic acid group, which bends towards the anatase in the un-solvated systems. Its spectra can be seen in Fig. 13d, and depicts the following: for systems I and II, hydrogen bonding to the anatase appears to have introduced a lower-frequency vibration around 50cm^{-1}, which is absent from the solvated cases. In systems II and IV, we see that dispersion enhances the peak at 750 cm^{-1}. It is also evident that the carboxylic acid stretching mode at 1720 cm^{-1} is enhanced significantly when both solvent and dispersion effects are present, in excellent accord with experiment (cf. Table 1).

[insert Fig. 9 here]

3.5 Titania Density of States

[insert Fig. 10 here]

PBE, like all GGA functionals, tends to under-estimate the band gap of anatase and our results, being no exception, agree closely with the work done by Martsinovich *et al*.[45] As can be seen in Fig. 10, the addition of dispersion has only a limited effect on the electronic structure of the anatase surface, where as the explicit inclusion of the RTIL solvent for systems III and IV, results in the HOMO, LUMO and Fermi levels being shifted by ~3 eV, an amount close in magnitude to that of the experimental band-gap itself (3.3 eV). Certainly, future work exploring the use of alternative functionals that can better predict band gaps and other electronic properties, including optimised range-separated hybrid functionals,[47] would help to disentangle these questions.

Concluding Remarks

This work has demonstrated the feasibility of simulating interfaces of this scale and complexity *via* ab-initio molecular dynamics.

The use of Grimme D3 dispersion corrections to the PBE functional does not seem to work well for adsorbed-chromophore interfaces *in vacuo*, which, by lacking some form of screening, results in an 'over-compensation' from the added corrections to the implicit dispersion already contained within the PBE functional, this has been discussed in various studies elsewhere.[43,44] Proceeding with dispersion corrections anyway can result in dramatically different structure and vibrations, which are artefacts of the simulations. Accounting for dispersion through the Grimme corrections when an explicit solvent is also included gives results that appear more physically realistic; the dispersion imparts to the liquid a more effective van der Waals interaction, and the liquid in turn, due to its dielectric environment, dampens the longer-range interactions of the interface coming from the additive dispersion corrections.

In so far as the calculated vibrational frequencies overlap with those available to experimental scrutiny and measurement, we have seen good agreement between the expected frequencies and those that we have calculated. An exception to this is that we did not see the expected symmetric stretch mode of carboxylate at 1380 cm^{-1}, instead seeing peaks belonging to carboxylate at 1330 and 1450 cm^{-1}. The latter frequency would possibly overlap with an experimental absorption spectrum for bipyridine. Although the interplay of dispersion and solvation effects on the vibrational dynamics of the interface is highly non-linear, the general trend tends to be that dispersion shifts vibrations to lower frequencies, and that solvation damps frequencies that are less than 1000 cm^{-1}.

Solvating the system with $[bmim]^+[NTf_2]^-$ has little corrosive effect on either the semiconductor or dye molecule and actually helps to stabilise the binding of the dye to the surface. When dispersion effects are also included, there are some structural changes but nothing too significant or unrealistic, with solvation effects clearly dominating those of dispersion. The cations are most affected by the inclusion of dispersion, followed by the anion, then the dye and lastly with almost no affect the anatase. We have seen that the N719 dye relaxes to a different geometry depending on whether it is solvated or not. This should serve as a caution for simulations which ignore the effect an explicit solvent has on an interface such as this. We have also seen that it is possible for these dyes *in vacuo* to undergo

changes to their binding modes spontaneously, and on the order of a picosecond. This could explain in part why determining unambiguously the exact binding mechanism has proved problematic in the past, as multiple binding modes might present themselves in a sample. Other studies have also seen spontaneous changes to the binding structure on the same timescale as this,[11] even when solvated with low-viscosity liquids, such as acetonitrile. For our systems solvated with a high-viscosity RTIL, we find this not to be the case, suggesting a relationship between the liquid and the stability of the adsorbed dye. Future work will examine how varying the liquid alters the behaviour of the interface.

Upon the inclusion of dispersion to the solvated system, the average separation between the cations and anions decreases by 0.6 Å. The average separation between the cations of the RTIL and the surface also decreases by 0.5 Å. With dispersion, the layering of the RTIL is significantly altered in the first layer surrounding the dye, with the cations being 1.5 Å further away than when dispersion is not included. The fact that dispersion plays such an important role in determining the layering structure of this ionic liquid indicates the importance of accurately capturing these interactions for reliable treatment of these ionic solvent environments with their strong local electric fields. As an important aspect of the operation of DSCs is charge regeneration of the hole by the electrolyte, it might be possible to engineer the layering of ionic liquids by the relative sizes of the anion and cation, such that the dye is surrounded by an optimal layer of hole acceptors. Naturally, further work would be required to address this challenging problem.

Supporting Information

(A) Additional structural g(r) plots for the solvated dye. (B) Additional structural $g(r)$ plots for the anion-dye interaction (C) Additional Vibrational Spectra of various species.

Acknowledgements

The authors thank Dr. Clotilde Cucinotta, Dr. Marco Masia and Dr. Pietro Ballone for useful discussions. This research has been supported by the Programme for Research in Third Level Institutions (PRTLI) Cycle 5 and co-funded by the European Regional Development Fund. We thank SFI, ICHEC and KAUST for the provision of high-performance computing facilities. We also wish to thank Prof. Adrian Ottewill and the UCD Simulation Science Programme, and the Erasmus Mundus Gulf Programme. This project has received funding from the European Union's Horizon 2020 research and innovation programme under grant agreement No. 643998.

References

1. Grätzel, M. Photoelectrochemical Cells. *Nature*, **2001.** 414
2. Hardin, B.E., Snaith, H.J. & McGehee, M.D., The Renaissance of Dye-Sensitised Solar Cells. *Nature Photonics*, **2012**. *6(3)*, 162–169.
3. O'Regan, B. & Grätzel, M., A Low-Cost, High-Efficiency Solar Cell based on Dye-Sensitised Colloidal TiO2 Films. *Nature*, **1991.** *353*, 737–740.
4. Hagfeldt, A. *et al*., Dye-Sensitised Solar Cells. *Chem. Rev.* **2010**, *110*, .6595–6663.
5. Kawano, R. *et al*., High performance Dye-Sensitised Solar Cells using Ionic Liquids as their Electrolytes. *J. Photochem. Photobiol. A*, **2004.** *164(1-3)*, 87–92.
6. Han, Y., Pringle, J. M. & Cheng, Y.-B. Improved Efficiency and Stability of Flexible Dye Sensitised Solar Cells on ITO/PEN Substrates Using an Ionic Liquid Electrolyte. *Photochem. Photobiol.* **2015**. *91***,** 315–22.
7. Wang, P., Zakeeruddin, S., Exnar, I. & Gratzel, M. High efficiency Dye-Sensitised Nanocrystalline Solar Cells based on Ionic Liquid polymer gel Electrolyte. *Chem. Commun.* **2002.** *5*, 2972–2973
8. Electrochemical Aspects of Ionic Liquids, Hiroyuki Ohno, John Wiley & Sons **2011**
9. Lee, K.E. *et al*., Further understanding of the Adsorption Mechanism of N719 sensitizer on anatase TiO2 films for DSSC applications using Vibrational Spectroscopy and confocal Raman imaging. *Langmuir*, **2010.** *26(12)*, 9575–83
10. Finnie, K. S., Bartlett, J. R. & Woolfrey, J. L. Vibrational Spectroscopic Study of the Coordination of Complexes to the Surface of Nanocrystalline Titania. *Langmuir* **1998.** *7463*, 2744–2749.
11. Suto, K., Konno, A., Kawata, Y., Tasaka, S. & Sugita, A. Adsorption dynamics of the N719 dye on nanoporous titanium oxides studied by Resonance Raman Scattering and Fourier transform Infrared Spectroscopy. *Chem. Phys. Lett.* **2012.** *536***,** 45–49.
12. Schiffmann, F., Vandevondele, J., Wirz, R., Urakawa, A. & Baiker, A. Protonation-dependent Binding of Ruthenium bipyridyl Complexes to the Anatase (101) surface. *J. Phys. Chem. C* **2010.** 8398–8404.
13. Angelis, F. De, Vitillaro, G., Kavan, L. & Nazeeruddin, Mohammad K. Gratzel, M. Modeling Ruthenium-Dye-Sensitised TiO2 Surfaces Exposing the (001) or (101) Faces: A First-Principles Investigation. *J. Phys. Chem. C* **2012.** *116*, 18124–18131.
14. S. Bandaru, N.J. English & J.M.D. MacElroy, Implicit and Explicit Solvent Models for modelling a bifunctional arene ruthenium Hydrogen-Storage Catalyst: a classical and *ab initio* Molecular Simulation Study, *J. Comput. Chem.*, **2014.** *35(9)*, 683-691

15. Almeida, K. J. De, Ramalho, T. C., Alves, M. C. & Vahtras, O. Theoretical Insights into the Visible Near-Infrared Absorption Spectra of Bis(hexafluoroacetylacetonate) copper(II) in Pyridine. Int. J. Quantum Chem. **2012.** *112*, 2571–2577

16. Mosconi, E., Selloni, A. & Angelis, F. De, Solvent Effects on the Adsorption Geometry and Electronic Structure of Dye-Sensitised TiO2: A First Principles Investigation. *J. Phys. Chem. C*, **2012.** *116*, 5932–5940.

17. Grimme, S., Semiempirical GGA-type Density Functional Constructed with a long-range Dispersion Correction. *J. Comput Chem*, **2006.** *27(15)*, 1787–1799.

18. Grimme, S. *et al*., A Consistent and Accurate ab initio parameterisation of Density Functional Dispersion Correction (DFT-D) for the 94 elements H-Pu. *J. Chem. Phys.*, **2010.** *132(15)*, 154104.

19. Izgorodina, E.I., Bernard, U.L. & MacFarlane, D.R., Ion-pair Binding Energies of Ionic Liquids: can DFT compete with ab initio-based methods? *The J. Phys. Chem. A*, **2009**. *113(25)*, 7064–72.

20. Castells, M.P.D.L., Stoll, H. & Mitrushchenkov, A.O., Assessing the Performance of Dispersionless and Dispersion-accounting Methods: Helium Interaction with Cluster Models of the TiO_2(110) Surface. *J. Phys. Chem.. A*, **2014.***110*

21. Hutter Jürg, Iannuzzi Marcella, Schiffmann Florian, VandeVondele Joost. cp2k: Atomistic Simulations of Condensed Matter Systems. WIREs Comput Mol Sci, **2014.** *4*, 15-25.

22. I.Bethune, A.Carter, X.Guo, P.Korosoglou:"Million Atom KS-DFT with CP2K", PRACE whitepaper, PRACE-1IP, pdf: http://www.prace-ri.eu/IMG/pdf/Million_Atom_KS-DFT_with_CP2K.pdf

23. Arita, M., Bowler, D. & Miyazaki, T. Stable and Efficient Linear Scaling First-Principles Molecular Dynamics for 10,000+ atoms. J. Chem. Theory **2014,** *10 (12)*, 5419–5425.

24. Angelis, F. De; Fantacci, S; Selloni, A; Nazeeruddin, M.K. and Graetzel, M., First Principles Modeling of the Adsorption Geometry and Electronic Structure of Ru(II) Dyes on Extended TiO_2 Substrates for Dye-Sensitised Solar Cell Applications. J. Phys. Chem. C **2010,** *114*, 6054-6061.

25. N. Martsinovich, D. R. Jones, A. Troisi, Electronic Structure of TiO2 Surfaces and Effect of Molecular Adsorbates J. Phys. Chem. C **2010,** *114*, 22659–22670.

26. Dragoni, D., Manini, N. & Ballone, P., Interfacial Layering of a Room-Temperature Ionic Liquid Thin Film on Mica: A Computational Investigation. *ChemPhysChem*, **2012,** *13(7)*, 1772–1780.

27. Angelis, F. De, Fantacci, S., Mosconi, E., Nazeeruddin, M. K. & Grätzel, M. Absorption Spectra and Excited State Energy Levels of the N719 dye on TiO2 in Dye-Sensitised Solar Cell models. *J. Phys. Chem. C* **2011,** *115*, 8825–8831.

28. Lippert,G., Hutter, J.,Parrinello ,M.,A Hybrid Gaussian and Plane Wave Density Functional Scheme. *Mol. Phys.,* **1997** *92 (3),*

29. VandeVondele, J. *et al*., Quickstep: Fast and Accurate Density Functional Calculations using a mixed Gaussian and Plane Waves Approach. *Comp. Phys. Comm.*, **2005.** *167(2),* 103–128.

30. VandeVondele, J. & Hutter, J., An Efficient Orbital Transformation Method for Electronic Structure Calculations. *J. Chem. Phys.*, **2003.** *118(10),* 4365.

31. Lippert, G., Hutter, J. & Parrinello, M., The Gaussian and Augmented-Plane-Wave Density Functional Method for ab initio Molecular Dynamics Simulations. *Theo. Chem. Acc.*, **1999.** 124–140.

32. Krack, M. & Parrinello, M., All-Electron ab initio Molecular Dynamics. *Phys. Chem. Chem. Phys.*, **2000,** *2,* 2105-2112.

33. Grotendorst, J., *High performance Computing in Chemistry*, NIC series 25 **2004,** http://hdl.handle.net/2128/2936

34. Hutter, J. *et al*., Cp2K: Atomistic Simulations of Condensed Matter Systems. *Wiley Interdisciplinary Reviews: Computational Molecular Science*, **2014.** *4(1),* 15–25.

35. Perdew,J.P., Burke,K. ,Ernzerhof,M., Generalised Gradient Approximation Made Simple , *Phys. Rev. Letter*, **1996,** *77(18)* 3865 - 3868.

36. Hoover, W. Canonical Dynamics: Equilibrium Phase-Space Distributions. *Phys. Rev. A* **1985,** *31***,** 1695–1697

37. M. P. Allen and D. J. Tildesley, Computer Simulation of Liquids, Oxford University Press, **1987**.

38. English, N. , Kavathekar, R. & MacElroy, J.M. Don. Hydrogen Bond Dynamical Properties of Adsorbed Liquid Water Monolayers with various TiO_2 Interfaces. Mol. Phys. **2012,** *110 (23)* 2919-2925

39. Binetti, E. & Panniello, A., Interaction of TiO2 Nanocrystals with Imidazolium-based Ionic Liquids. *J. Phys. Chem. C,* **2013,** 2–8.

40. Forero-Martinez, N. C., Cortes-Huerto, R. & Ballone, P. The glass Transition and the Distribution of Voids in Room-Temperature Ionic Liquids: a Molecular Dynamics Study. *J. Chem. Phys.* **2012,** *136,* 204510

41. Troncoso, J., Cerdeirina, A. C., Sanmamed, A. Y., Romani, L. & Rebelo, L. P. N. Thermodynamic properties of Imidazolium-Based Ionic Liquids: densities, heat capacities, and enthalpies of fusion of and. *J. Chem. Eng. Data,* **2006,** *51,* 1856–1859.

42. Pópolo, M. Del, Lynden-Bell, R. M. & Kohanoff, J. Ab initio Molecular Dynamics Simulation of a Room Temperature Ionic Liquid. *J. Phys. Chem. B* **2005,** *109,* 5895–5902.
43. Kim, H., Choi, J.M. , Goddard, W. A. Universal Correction of Density Functional Theory to include London Dispersion (up to Lr, element 103). *J. Phys. Chem. Lett.* **2012,** 3, 360–363.
44. Izgorodina, E. , Bernard, U. L. & MacFarlane, D. R. Ion-pair binding energies of Ionic Liquids: can DFT compete with ab initio-based Methods? *J. Phys. Chem. A,* **2009,** *113,* 7064–72.
45. Martsinovich, N., Jones, D. R. & Troisi, A. Electronic Structure of TiO_2 Surfaces and Effect of Molecular Adsorbates Using Different DFT Implementations. *J. Phys. Chem. C* **2010.** *114,* 22659–22670.
46. Thomas, M., Brehm, M., Fligg, R., Vöhringer, P. & Kirchner, B. Computing Vibrational Spectra from ab initio Molecular Dynamics. *Phys. Chem. Chem. Phys.* **2013** *15,* 6608–22.
47. Refaely-Abramson, S. Jain, M., Sharifzadeh, S., Neaton, J.B., Kronik, L. Solid-state optical absorption from optimally tuned time-dependent range-separated hybrid density functional theory, *Phys. Rev. B* **2015**, *92*, 081204.

Table 1: Main experimental peaks present in the infra-red absorption spectra of N719/0TBA dye adsorbed onto anatase. [10,11]

Frequency (cm^{-1})	Established Mode
1380	Symmetric COO^- stretching of carboxylate
1450	Bipyridine stretching mode
1491	Bipyridine stretching mode
1540	C=C modes of bipyridine rings
1563	Bipyridine stretching mode
1600	Anti-symmetric COO^- stretching of carboxylate
1608	Bipyridine stretching mode
1720	C=O stretching of carboxylic acid
2100	N-C thiocyanate stretching mode

Figure list

1. Various binding modes possible for the N719 molecule (reprinted with permission from Lee, K.E. *et al*., 2010).[9]
2. Atomistic representation of the N719 dye bound to the titania surface. The left hand side is bound via bidentate bridging, while the right hand side is monodentate. Labelling is as follows; $C_{a,b,c,d}$ are the carbon atoms of the carboxyl groups, $O_{e,f,g,h}$ are the oxygen atoms of the two carboxylates, Ru_i is the single ruthenium atom at the centre of the N719 dye, $S_{j,k}$ are the sulphur atoms of the two thiocyano groups. $Py_{l,m,n,o}$ are the four pyridine rings of the N719 dye. C_a is hidden from view.
3. Typical simulation cell set-up. The anatase surface is shown in grey, the N719 dye in white, bmim cations are in blue and NTf_2 anions in red. The mesh indicates a typical van der Waals radius around the liquid molecules.
4. (a) Initial starting configuration of the dye for all four simulations. (b) Configuration after 8.5 ps in un-solvated case without explicit dispersion (system I). For a discussion of why the highlighted carboxylic acid bends towards the anatase, consult main text and see Fig. 5.
5. $g(r)$ for hydrogen atoms in N719 and the oxygen atoms in the anatase surface, averaged over 1 to 2 ps (continuous red line) and 7.5 to 8.5 ps (dashed blue line shifted upwards for ease of viewing). (a) System I: The peak at 1.7 Å visible in the later snapshot between 7.5 ps and 8.5 ps is due to the bending of one of the carboxylic acids towards the surface and its subsequent physisorption binding to it, as seen in the insert. (b) System III: explicit solvation has resulted in a different relaxed geometry than system I, with no bending taking place.
6. Side view of the configuration of system II at different times in its dynamics trajectory; surface hydrogen atoms are emphasised in black. (a) Initial configuration and the same as the one shown in Fig. 4a. On the near-side of the dye, we can see the bidentate bridging while the far-side is monodentate. (b) Configuration after 1.5 ps. Proton-transfer from the surface has occurred on the far-side of the dye, altering the monodentate bridge. The bending of the carboxylic acid can also be seen. (c) Configuration after 8.5 ps. A near-side carboxylate oxygen has broken its chemical bond and rotated through a semi-circular arc.
7. $g(r)$ for ions in the RTIL and the titanium atoms in the anatase surface, averaged over 1 to 2 ps (continuous red line) and 7.5 to 8.5 ps (dashed blue line shifted upwards for ease of viewing). (a) system III: distribution of bmim cations with titanium atoms in the anatase (b) system IV: distribution of bmim cations and titanium atoms in the anatase, note the

closer proximity of the cations and surface due to the dispersion corrections (c) system III: distribution of Ntf_2 anions and titanium atoms in the anatase (d) system IV: distribution of Ntf_2 anions and titanium atoms in the anatase.

8. $g(r)$ for ions in the RTIL and the ruthenium atom in the dye, averaged over 1 to 2 ps (continuous red line) and 7.5 to 8.5 ps (dashed blue line shifted upwards for ease of viewing). (a) system III: distribution of bmim cations with the ruthenium atom of the dye (b) system IV: distribution of bmim cations with the ruthenium atom of the dye, note the significant reordering of the layers compared with system III (c) system III: distribution of Ntf_2 anions with the ruthenium atom of the dye (d) system IV: distribution of Ntf_2 anions with the ruthenium atom of the dye (e) system III: distribution of bmim cations and Ntf_2 anions (f) system IV: distribution of bmim cations and Ntf_2 anions, the cations and ions are closer on average by 0.6 Å than in system III .
9. Frequency spectra plotted against intensity for the four carbon atoms labelled $C_{a,b,c,d}$ in Fig. 2. **Upper panels:** Green continuous line represents system I, no solvation, no dispersion. Black dashed line denotes system II, no solvation, with dispersion. **Lower panels:** Red continuous line represents system III, with solvation, no dispersion. Blue dashed line denotes system IV, with solvation, with dispersion. (a) C_a: solvation inhibits carboxylic stretch mode at 1720 cm^{-1}. (b) C_b: solvation enhances frequency mode at 750 cm^{-1}. (c) C_c: higher frequency modes missing from system II due to alteration of binding mode. (d) C_d: systems I and II shows very low-frequency modes at 50 cm^{-1} due to hydrogen bonding to the anatase.
10. Density of states plotted against energy for each of the four systems. From top to bottom the green line denotes system I, the black line system II, the red line system III and the blue line system IV. The vertical lines denote the location of the Fermi level for each respective simulation. We note that upon addition of an explicit solvent the HOMO and LUMO levels end up being shifted by ~3 eV.

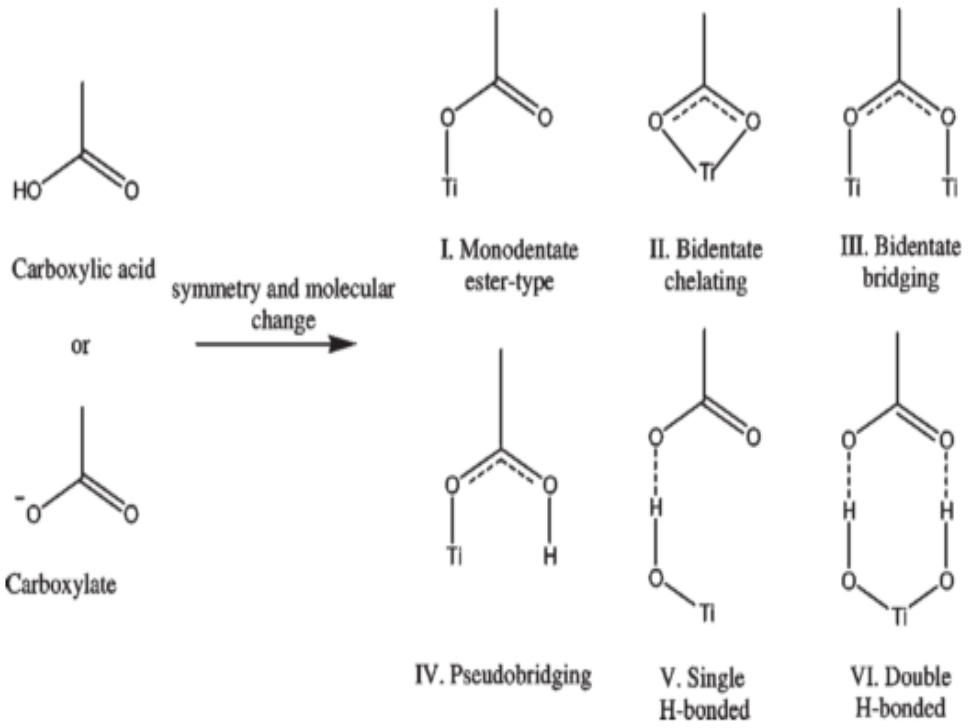
HO
O
Carboxylic acid
or
O
O
Carboxylate
symmetry and molecular change
O
O
Ti
I. Monodentate ester-type
O
O
Ti
II. Bidentate chelating
O
O
Ti
Ti
III. Bidentate bridging
O
O
Ti
H
IV. Pseudobridging
O
O
H
O
Ti
V. Single H-bonded
O
O
H
H
O
O
Ti
VI. Double H-bonded

Fig. 1

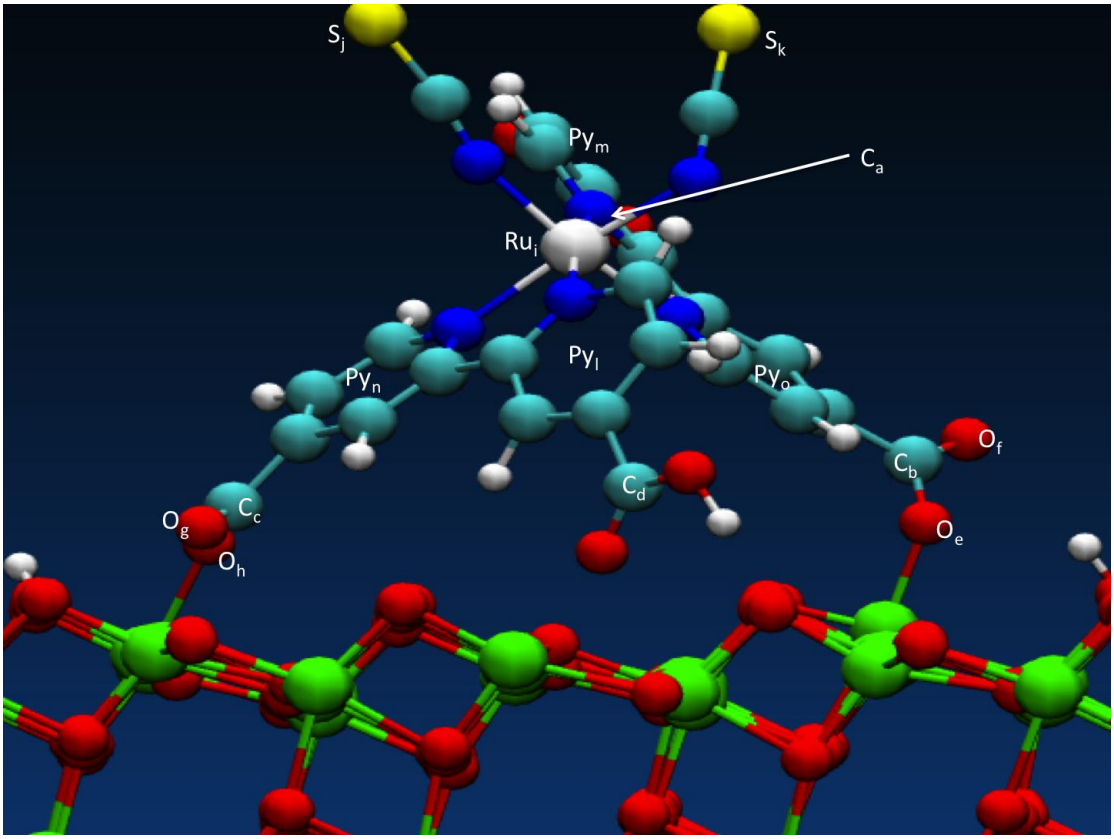

Fig. 2

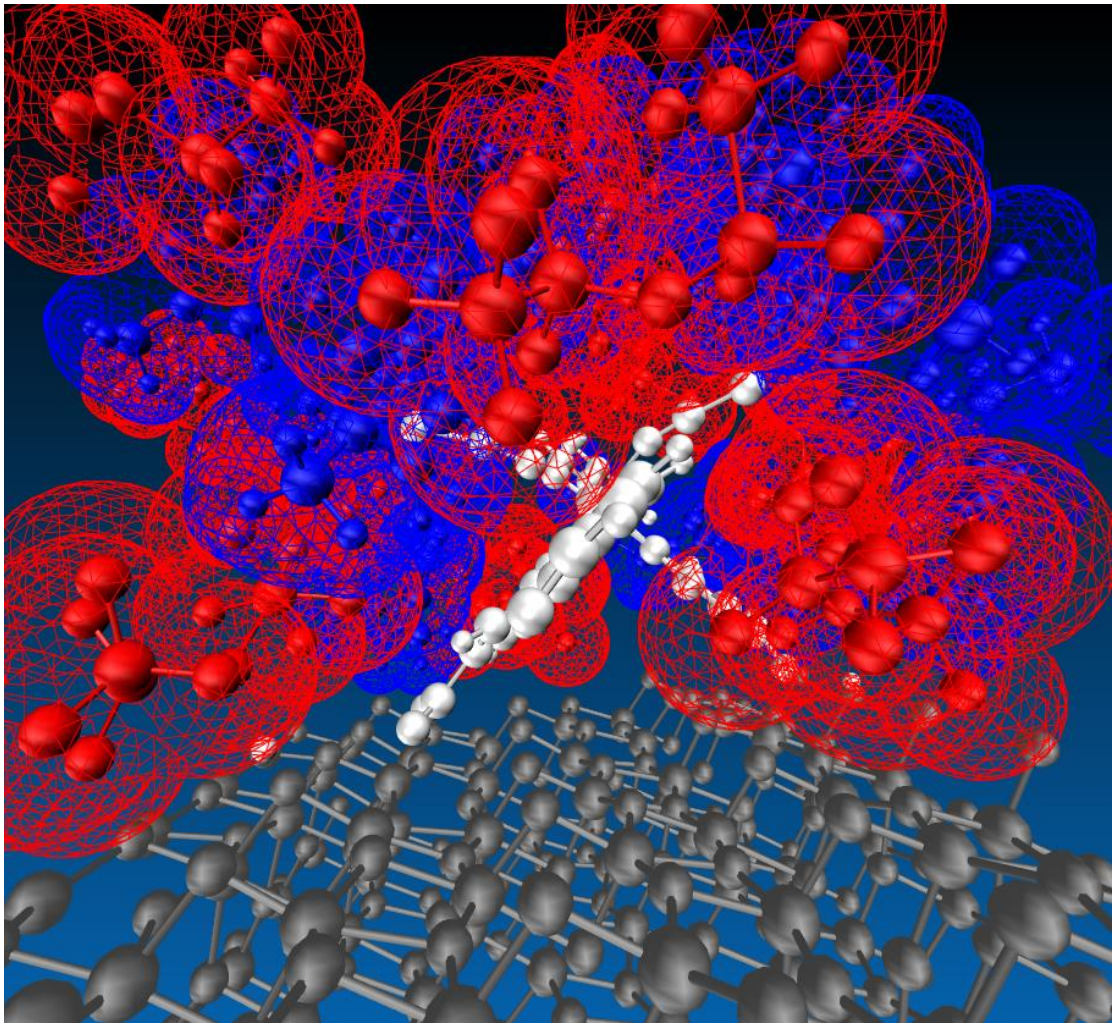

Fig. 3

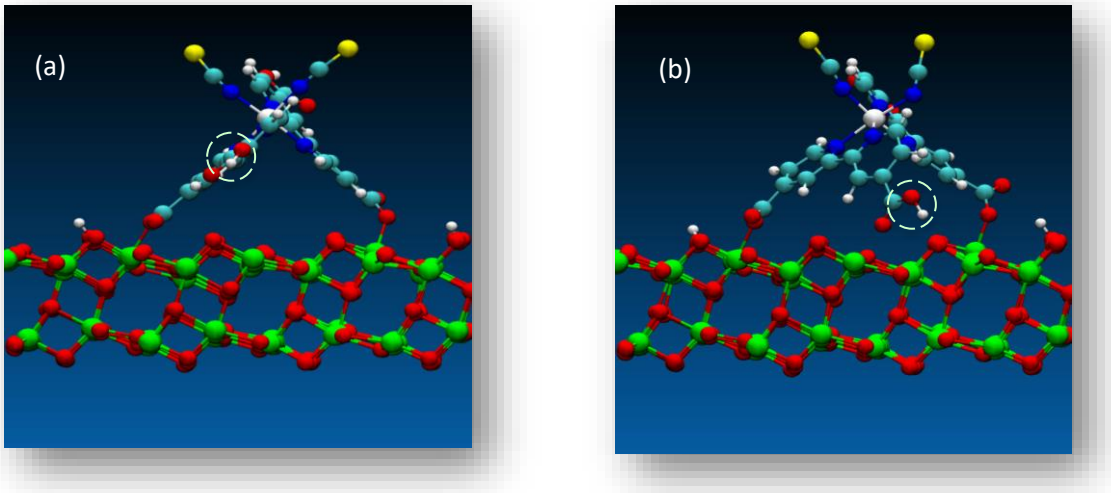

Fig. 4

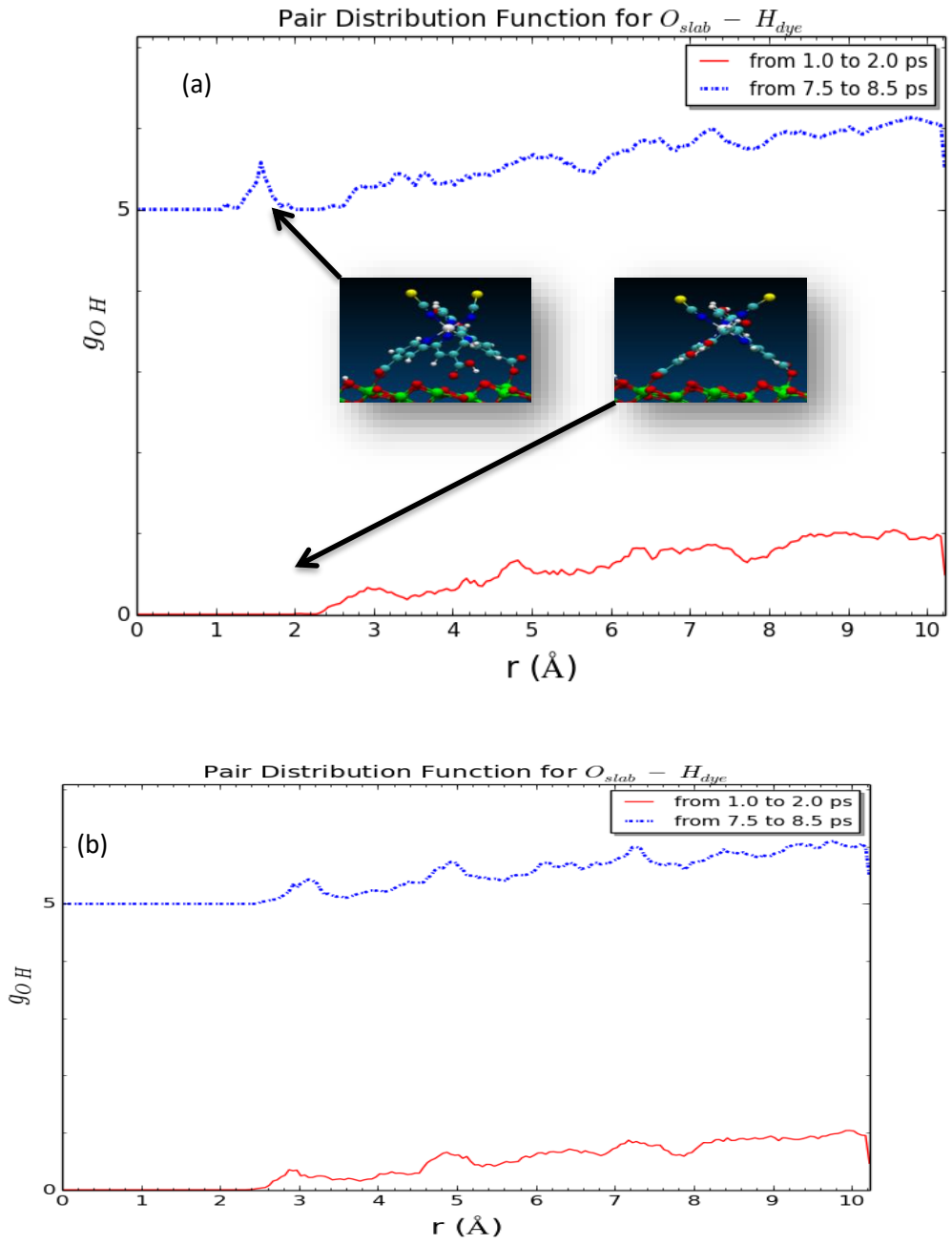
Pair Distribution Function for O_{slab} – H_{dye}
(a)
from 1.0 to 2.0 ps
from 7.5 to 8.5 ps
$g_{O\,H}$
r (Å)
Pair Distribution Function for O_{slab} – H_{dye}
(b)
from 1.0 to 2.0 ps
from 7.5 to 8.5 ps
$g_{O\,H}$
r (Å)

Fig. 5

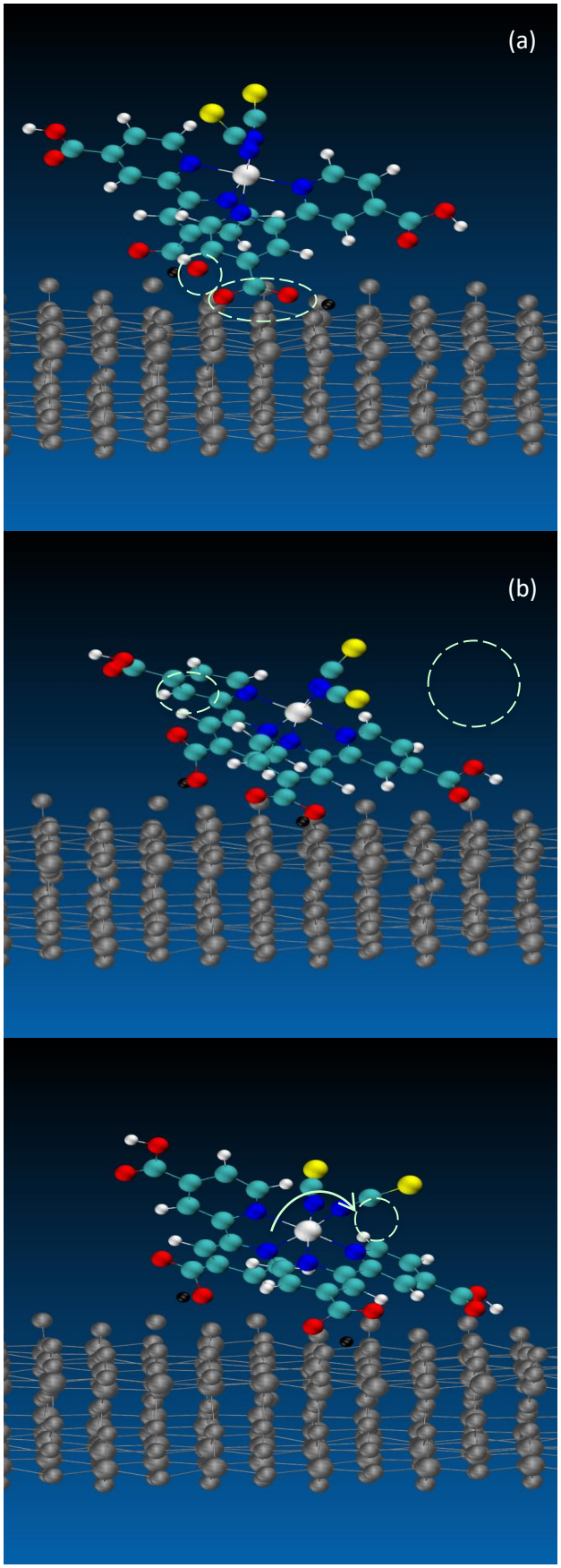

Fig. 6

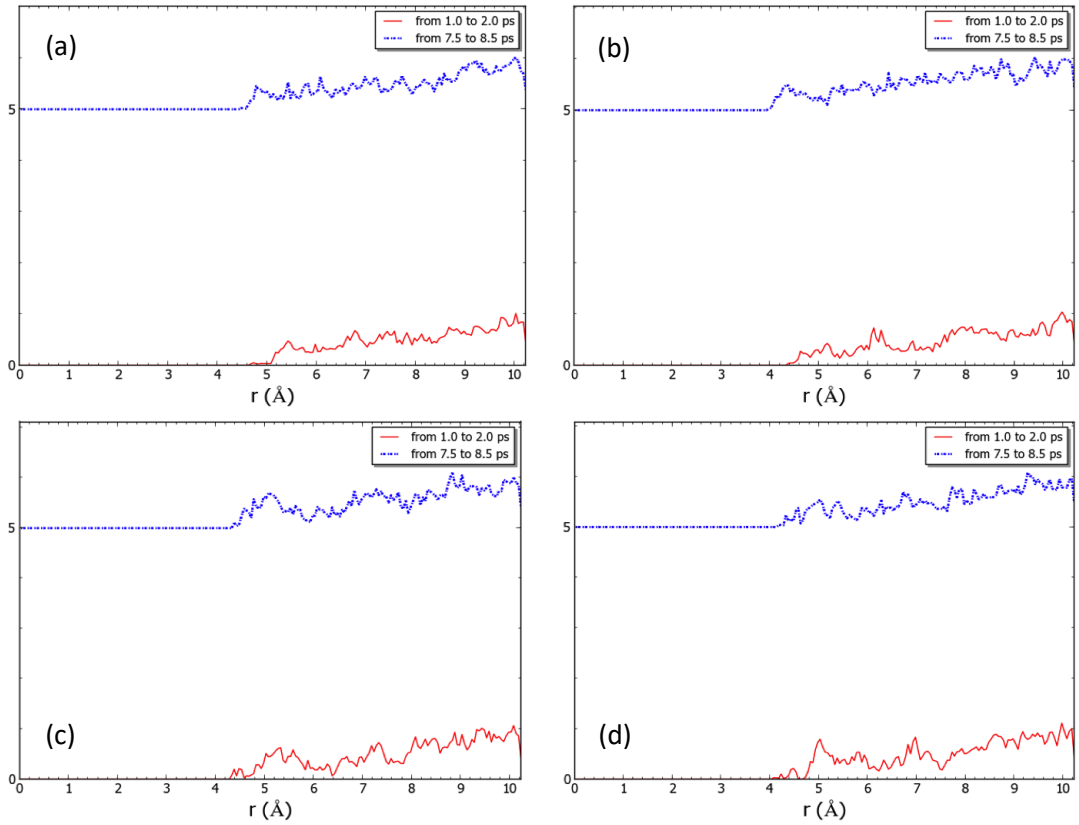

Fig. 7

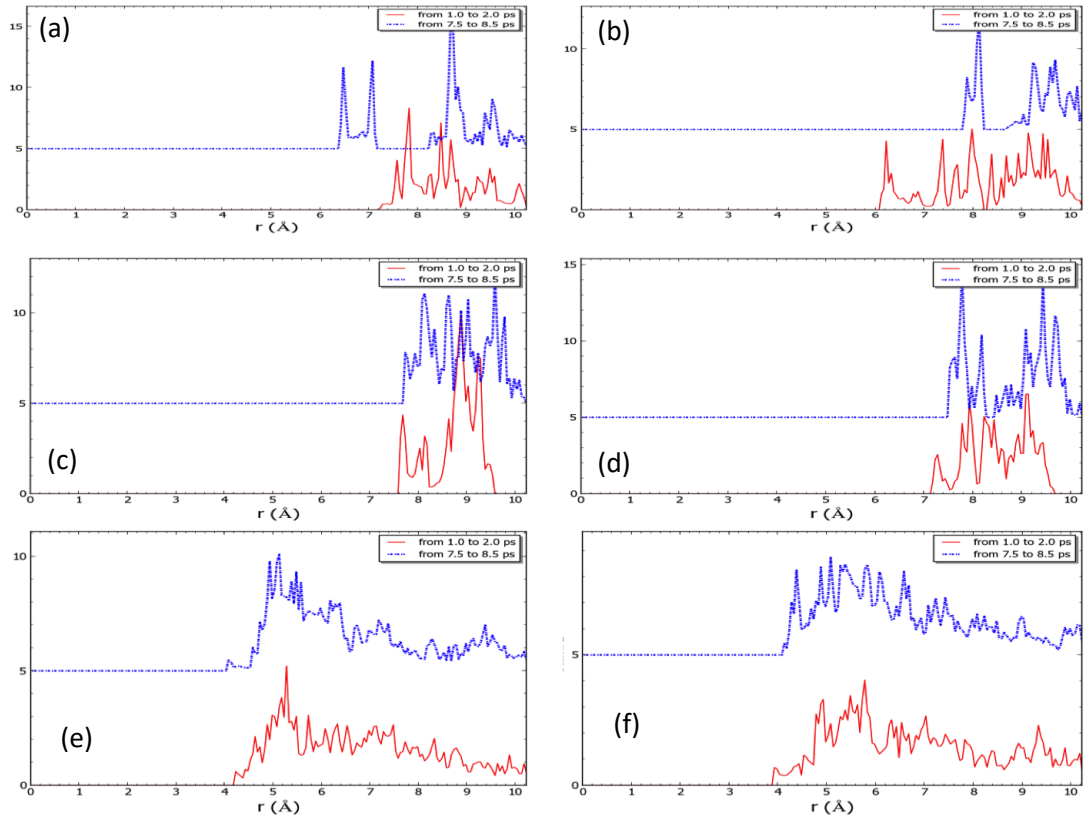

Fig. 8

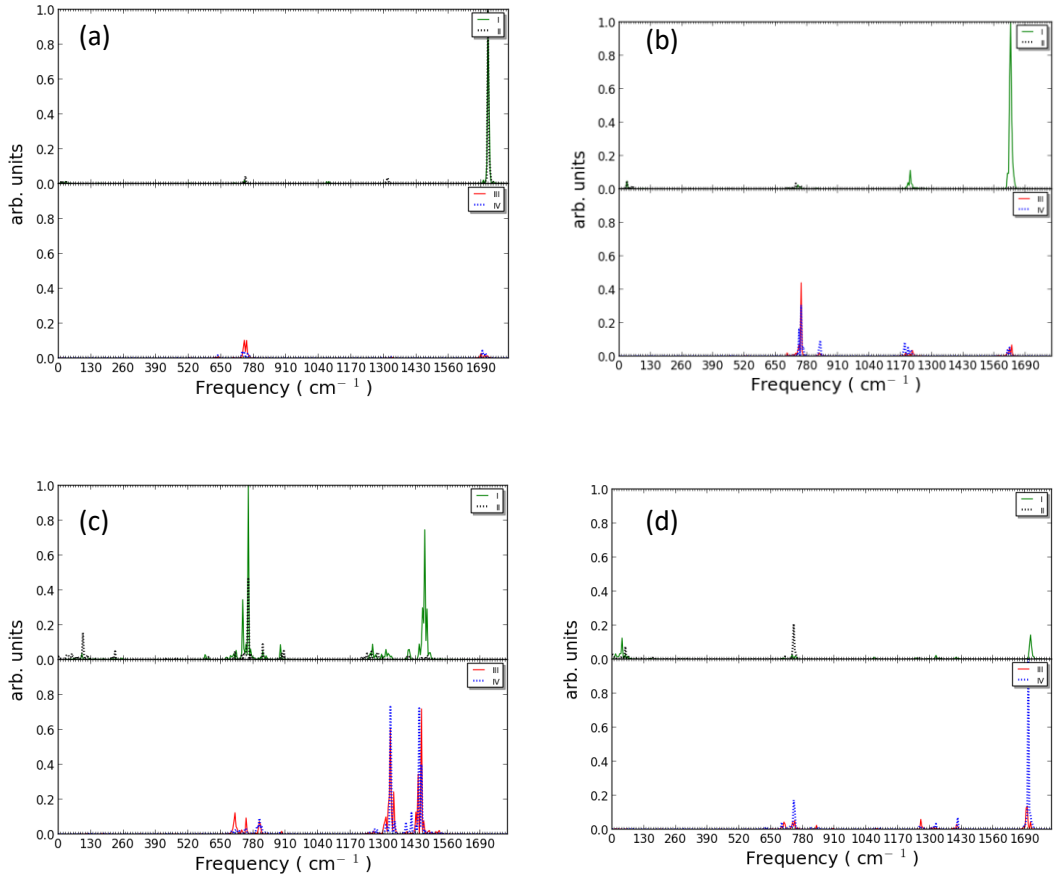
(a)
(b)
(c)
(d)
arb. units
Frequency (cm^{-1})
0 130 260 390 520 650 780 910 1040 1170 1300 1430 1560 1690
0.0 0.2 0.4 0.6 0.8 1.0
I
II
III
IV

Fig. 9

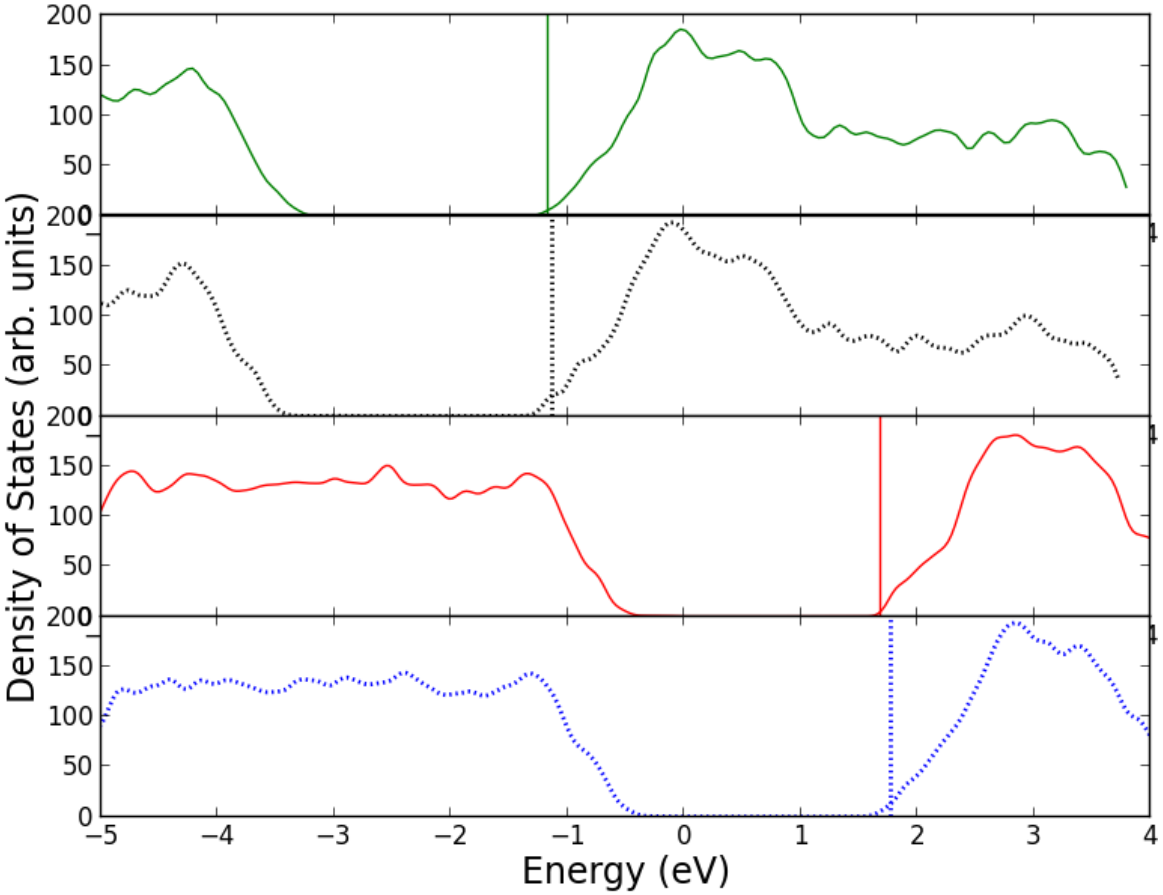
Density of States (arb. units)
Energy (eV)
200
150
100
50
0
−5
−4
−3
−2
−1
0
1
2
3
4

Fig. 10